Effects of Laser Spot Distance on Production Rate of Carbon Nanostructure Synthesis with Laser Ablation in Liquid using Nanosecond Pulse Lasers

Kresna Budiman[1], Wahyu Erlangga[1], Leonard Sean[1], Ichanul Taqwim[1], and Heru Santoso B. Rochardjo[1,*]

[1)]Department of Mechanical and Industrial Engineering, Universitas Gadjah Mada, Indonesia

Corresponding Author's email: heru-sbr@ugm.ac.id

Abstract. Laser ablation in liquid has become increasingly more popular due to it's short preparation time, no need for hazardous chemicals, a wide selection of nanomaterials , and it's properties that can be easily tuned by adjusting parameters in the ablation process. This research compares the production rate of this synthesis process between variations of spatial distances between laser pulse spots at the target, which is varied by controlling the galvo scanning speed of the laser system. Variations of galvo scan speeds include: 250, 500, 1000, 2500, 5000, and 10000 mm/s. The production yield of each scan speeds are compared by measuring the absorbance of the synthesized colloids with UV- VIS spectrophotometry. Results showed that the ablation process with a scan speed of 2500 mm/s has the highest production rate.

Keywords: Nanomaterials, Galvo Speed, Laser Ablation, Carbon Nanostructure, Graphite.

1 INTRODUCTION

In recent years, carbon nanostructures such as graphene has become one of the most promising materials due to it's physical, mechanical, electrical, and chemical properties. Graphene has found it's use in various applications, such as external stimuli based drug delivery systems for cancer therapy [1], water purification membranes [2][3], electronics and solar cells [4], [5], biosensors [6], and structural reinforcement [7]. Various methods are used to produce graphene and graphene oxide, such as chemical vapor deposition (CVD), chemical exfoliation, electrochemical exfoliation, epitaxial growth, liquid phase exfoliation, and mechanical exfoliation[8]. Laser ablation in liquid is chosen in this paper due to it's low preparation time, relatively cheap and non-hazardous materials, and the absence of toxic or hazardous by products [9], [10]. Generally, this method produces nanomaterials by generating a plasma plume and a cavitation bubble at the surface of the target material using a pulsed laser. This cavitation bubble containing the plasma plume is then quenched by the surrounding liquid medium, resulting in rapid cooling (quenching) of the ablated target material and inducing a shock wave [11]. This combination of thermal and mechanical action breaks the weak Van der Waals bond between graphite layers, resulting in the release of carbon nanomaterials into the medium [12].

M. A. Muflikhun et al. (eds.), *Proceedings of the 10th International Conference on Science and Technology (ICST 2024)*, Advances in Engineering Research 268,
https://doi.org/10.2991/978-94-6463-772-4_40

Previous researches have used various different laser systems, in which some used lasers with relatively low pulse repetition rates (around 10Hz or less), while others use higher repetition rates (>1kHz). The pulse duration and energy of these previous researches also vary[13]–[21]. Increasing the repetition rate of the laser may increase the production rate of the nanomaterials, however this will also result in the reduction of efficiency due to the formation of plasma and cavitation bubbles at the surface of the target material. This plasma plume acts as a shield throughout it's lifetime, preventing the next laser pulse from reaching the target material [22]. This issue can be addressed by spatially separating the pulses, by passing the plasma plume before the end of it's lifetime. However, the size and lifetime of these plasma plumes vary with different laser pulse energies and pulse durations[23]. The majority of researches regarding of laser ablation in liquid use laser systems with pulse durations shorter than 10 nanoseconds. Meanwhile, these laser systems tend to be costly, with femtosecond pulsed lasers ranging from $10,000.00 up to $250,000.00. The viability of laser systems with much longer pulse durations (~100ns), a galvanometer for beam guiding method, and with repetition rates in the kilohertz range such as in lasers for marking and engraving purposes have not been thoroughly researched. With the hypothesis of cavitation bubbles growing larger with longer pulse durations, this research aims to investigate the viability of such lower-cost systems and identify problems occurring during the production process. This research also hopes to help providing information on things to be considered when utilizing similar laser systems, and how to optimize the parameters (specifically the spot distances) for nanomaterial production.

2 EXPERIMENTAL METHODS

2.1 Materials and Equipment

Graphite target pellets (10 mm diameter, 4 mm thick) are prepared from graphite rods using a mini lathe/CNC training unit (EMCO TU-2A). Targets are then submerged in 20mm column of distilled water in a wide-mouth, small container. A galvo laser (RAYCUS 30W, NdYAG-1064nm) is used to ablate the target. The laser has a gaussian beam with a spot diameter of 0,05mm, with an average pulse duration of 135 nanoseconds.

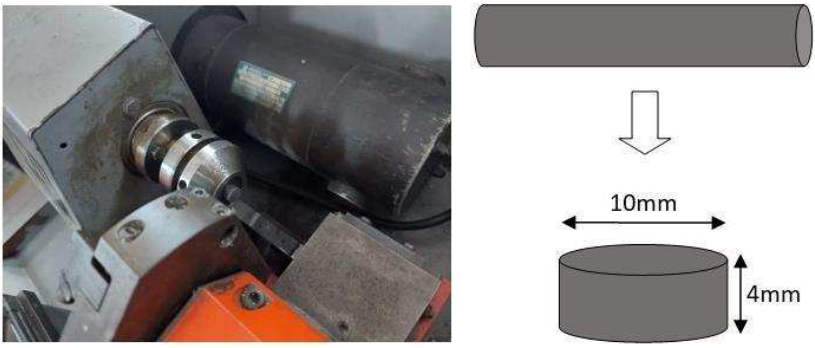

Fig. 1. Target preparation using a CNC training unit.

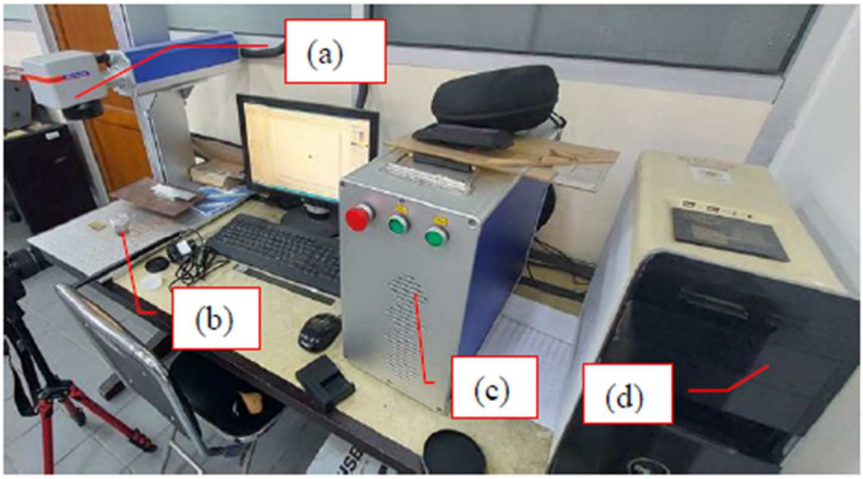

Fig. 2. Positioning of galvo scanner (a), sample (b), laser source (c), and computer (d) in the ablation setup**.**

The weight of the sample, medium, and target is measured. Targets are then submerged in 20 mm column of distilled water as liquid medium. All samples are sonicated for 5 minutes to help reduce the amount of air bubbles trapped inside the graphite targets. Targets are then irradiated with the laser for 5, 10, and 20 minutes. The laser is set to maximum continuous power (30W) and the pulse repetition rate is set to 20 kHz for all samples. Six variations of beam travel speed (250, 500, 1000, 2500, 5000, 10000 mm/s) are used to compare between spot distances. The beam travel is guided with a galvanometer head. A spiral pattern is used as beam guidance path.

The distance between spots are calculated using the formula:

$$D = \frac{S}{f} - d \tag{1}$$

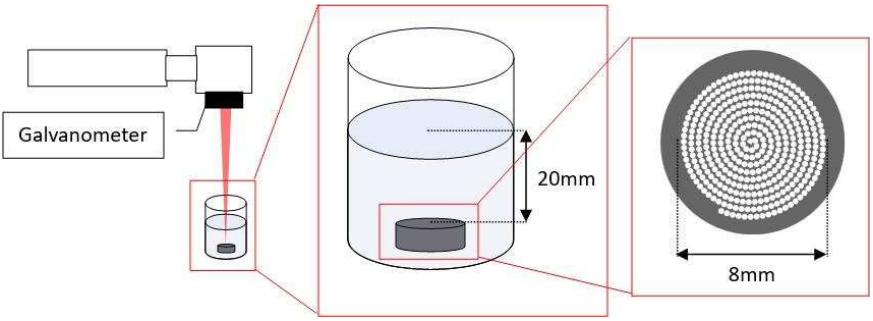

Fig. 3. Illustration of the ablation process setup, and beam travel path along the target.

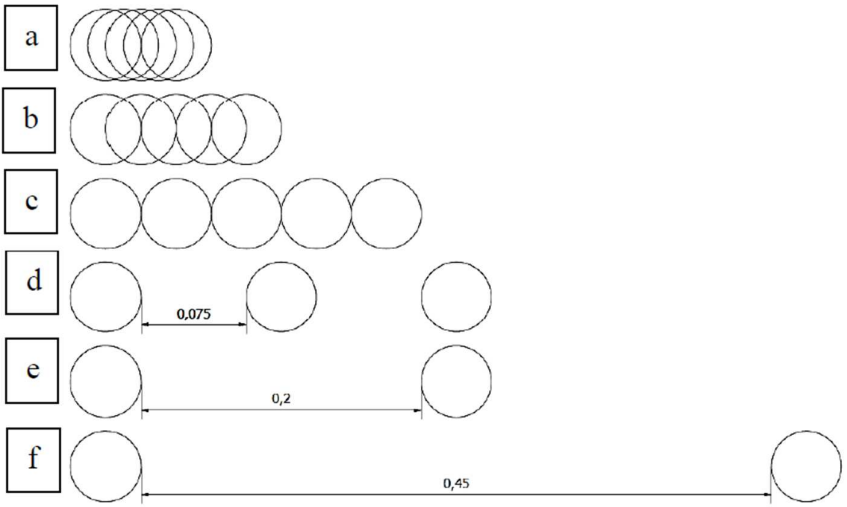

Fig. 4. Illustrations of spot positions with galvo speeds of 250 (a), 500 (b), 1000 (c), 2500 (d), 5000 (e), and 10000 (f) mm/s.

In which D is the distance between laser spots, S is the beam travel speed, f is the pulse frequency, and d is the spot diameter. When the spot distances are calculated using formula in Eq. 1, the spot distances tested in this experiment are: -0,0375; -0,025; 0; 0,075; 0,2; and 0,45mm. Negative values of these spot distances indicate that the adjacent spots are overlapping against each other, as shown in Figure 4.

The graphene solution is then transferred into a test tube for UV-VIS spectrophotometry to determine the concentration of carbon nanostructures present in the medium. Final liquid medium temperature is measured right after irradiation for

each samples using a thermogun. Each variation of the samples are repeated three times. The mean values of the peak absorption values and liquid medium temperatures are then calculated to compare between spot distances.

3 RESULTS AND DISCUSSIONS

The UV-VIS absorption spectra is presented in Figure 5. The absorption spectra show peak values around 320nm wavelengths. This is due to plasmonic absorption resonance in the free electron cloud of carbon materials (π- electrons). The graphs show that the peak absorption values of the samples generally increase with the increase of ablation time and galvo scan speed up to 2500 mm/s. However, samples that are made with galvo speeds of 250, 500, and 1000 mm/s show little to no increase of absorptivity over ablation time after 10 minutes, indicating that the production has stopped after ten minutes of continuous ablation.

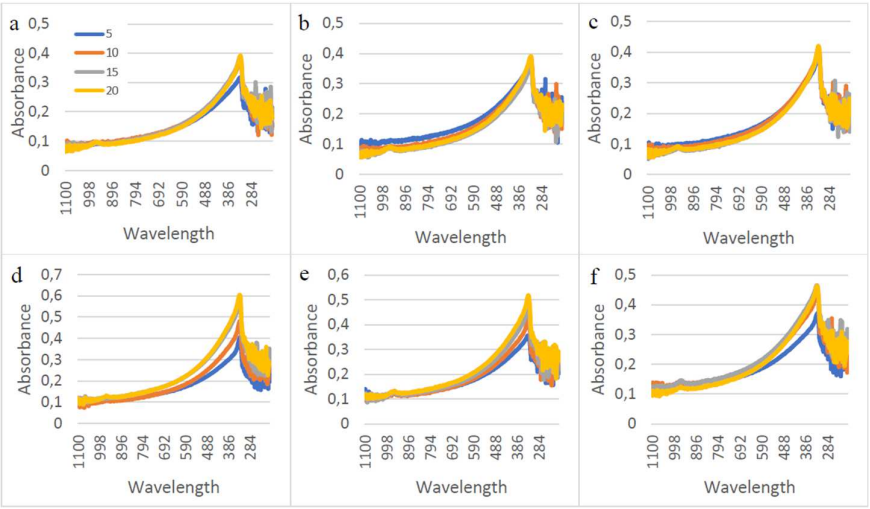

Fig. 5. UV-VIS absorption spectra of samples ablated with 250 (a), 500 (b), 1000 (c), 2500 (d), 5000 (e), and 10000 (f) galvo scan speeds.

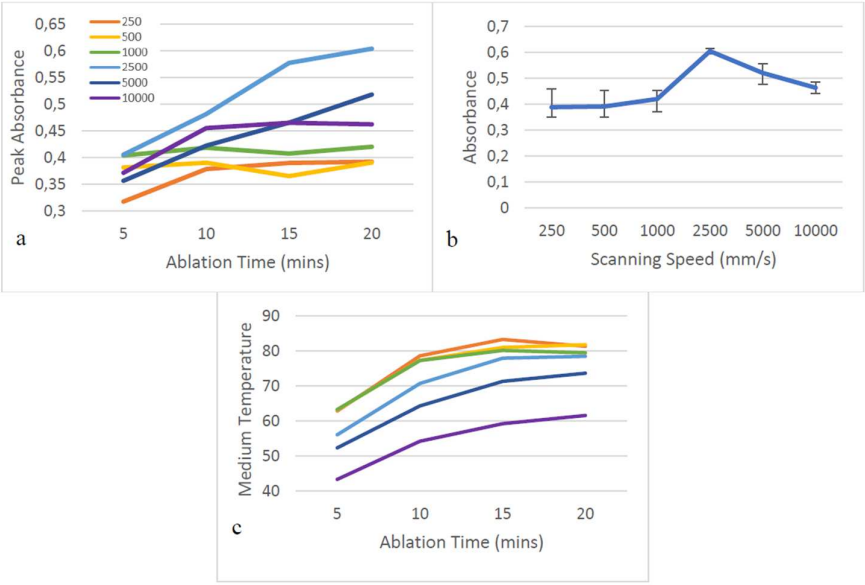

Fig. 6. Data summary of average peak UV-VIS absorbance values on all ablation time variations (a), after 20 mins of ablation time (b), and liquid medium temperature on different galvo scan speeds (c).

Table 1. Average peak absorption values and standard deviation on each time and scanning speed variations

Time	Scan Speeds (mm/s)											
	250		500		1000		2500		5000		10000	
(min)	Abs	Stddev	Abs	Stddev	Abs	Stddev	Abs	Stddev	Abs	Stddev	Abs	Stddev
5	0,32	0,15	0,38	0,12	0,40	0,11	0,41	0,04	0,36	0,01	0,37	0,03
10	0,38	0,08	0,39	0,11	0,42	0,14	0,48	0,04	0,42	0,05	0,46	0,08
15	0,39	0,05	0,37	0,04	0,41	0,18	0,58	0,01	0,47	0,04	0,47	0,05
20	0,39	0,12	0,39	0,11	0,42	0,08	0,60	0,01	0,52	0,06	0,46	0,04

The temperature graph also shows a correlation with the increase of absorptivity, specifically on galvo speeds below 2500mm/s. The medium temperature of these particular samples rise up to around 75-80°C and remains constant after 10 minutes. A footage taken during the production process shows that after these temperatures have been reached, the laser beam becomes unfocused as it reaches the target material, as shown on Figure . This phenomenon also introduces inconsistency in the ablation process, increasing the standard deviation of the peak absorption values, as shown on Table 1.

This phenomenon of unfocused laser beam can be attributed to the medium temperature during the production process. It can be observed on Figure 7 that the laser beam starts to induce a phase change (generating steam bubbles) before the laser beam is able to reach the target. The phase change of the medium drastically changes the

density and the refraction index of the medium along the beam path towards the target, inducing a case of thermal blooming [24]. This phenomenon results in the scattering of the laser beam, reducing the fluence below the ablation treshold of graphite which is about 185 mJ/cm^2(1,85 mJ/mm^2) [25]. The fluence of the laser beam can be calculated using formula in Eq. 2:

$$F = 2\frac{E}{\pi r^2} \tag{2}$$

In which F stands for the fluence of the laser beam, E stands for the laser energy on each pulse, and r for the spot radius of the laser beam. Since the laser beam used in this research has a gaussian profile, the laser fluence is multiplied by a factor of two.

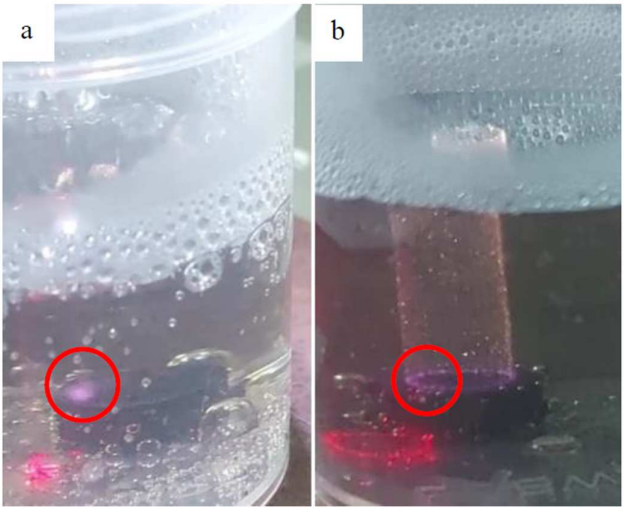

Fig. 7. Footage snapshot of the production process. Sample is irradiated with 250mm/s (a) and 10000mm/s (b) galvo scan speeds. The unfocused beam is shown in the red circle.

When the laser is fully focused towards the target, the laser has a beam fluence of 1,52 J/mm^2 (152 mJ/mm^2). Meanwhile the energy of the beam that successfully passes through the liquid medium can be calculated using Beer- Lambert law[26]:

$$I = I_0 e^{-(kx)} \tag{3}$$

In which I stands for the intensity or fluence of the beam reaching the target, I0 stands for the intensity or fluence of the beam prior to entering the medium, k being the absorption coefficient (0,135 cm^{-1} @ 25°C [27]), and x being the length of path traveled by the beam through the medium. With this formula, we get that the fluence of the beam reaching the target prior to thermal blooming is about 1,16 J/mm^2 (116 mJ/mm^2), which is still above the ablation treshold of graphite. However, when thermal blooming starts to occur, we can infer from the snapshot of the footage that the beam diameter expands to roughly 2mm wide. By recalculating the fluence of the laser beam we get

0,000955J/mm^2(0,0955mJ/mm^2) (without considering the absorption of water column), and 0,0729mJ/mm^2 when reaching the target, considering the absorption of water column, which gets far below the ablation treshold of the graphite target. This explains how the nanomaterial production stopped after 10 minutes on 250, 500, and 1000mm/s galvo speeds.

It is also worth noticing that the medium temperatures of samples with higher galvo speeds tend to be lower than samples ablated with slower galvo speeds. This indicates that the spatial bypassing of the plasma plume successfully reduces the amount of laser energy scattered and absorbed into the liquid medium, increasing the power efficiency and effectiveness of the production process.

The reduction of production yield on scanning speeds above 2500 mm/s can be attributed to the increase of distance between the laser spot to the heat affected zone (HAZ) generated from previous laser pulses on the target's surface, as illustrated on Figure 8. A study from Wagener et. al. shows that the increase of interpulse distances after bypassing the cavitation bubble will reduce the production yield of nanomaterials on each pulse. The heat affected zone generated from previous pulses aids in reducing the required energy for the next pulse to ablate the target, which increases the ablation yield of the next pulse. Bypassing the generated heat affected zone will diminish the energy requirement reduction, which decreases the ablation yield on each pulse [28].

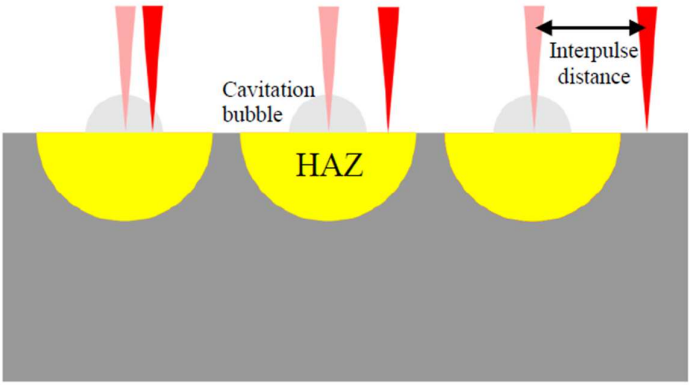

Fig. 8. Illustration of different interpulse distances and laser pulse positions related to cavitation bubble and HAZ formed by previous laser pulses.

4 CONCLUSION

This research aims to study the effects of laser spot distances towards the production rate of carbon nanostructures, along with identifying the problems occurring during the production process. According from the results, it can be concluded that increasing the beam travel speed (galvo speed) of the process up to 2500 mm/s results in higher production rate of nanomaterials. Production rate of nanomaterials then starts to decrease on higher scanning speeds. Increasing the beam travel speed will also reduce the energy lost and dissipated towards the liquid medium, reducing the medium

temperature. The increase of liquid medium temperature increases the chance of phase change of the medium along the beam path, scattering the laser beam and significantly reduces the laser fluence hitting the target material.

Acknowledgments. The article is a part of research supported by the Directorate of Research, Universitas Gadjah Mada under RTA Program 2023 with assignment number of 5075/UN1.P.II/DIT-LIT/PT.01.01/2023.

References

1. K. Yang, L. Feng, and Z. Liu, "Stimuli responsive drug delivery systems based on nano-graphene for cancer therapy," *Adv. Drug Deliv. Rev.*, vol. 105, pp. 228–241, Oct. 2016, doi: 10.1016/J.ADDR.2016.05.015.
2. J. Abraham *et al.*, "Tunable sieving of ions using graphene oxide membranes," *Nat. Nanotechnol. 2017 126*, vol. 12, no. 6, pp. 546–550, Apr. 2017, doi: 10.1038/nnano.2017.21.
3. D. Cohen-Tanugi and J. C. Grossman, "Water desalination across nanoporous graphene," *Nano Lett.*, vol. 12, no. 7, pp. 3602–3608, Jul. 2012, doi: 10.1021/NL3012853/SUPPL_FILE/NL3012853_SI_001.PDF.
4. A. M. Ilyas, M. A. Gondal, U. Baig, S. Akhtar, and Z. H. Yamani, "Photovoltaic performance and photocatalytic activity of facile synthesized graphene decorated TiO2 monohybrid using nanosecond pulsed ablation in liquid technique," *Sol. Energy*, vol. 137, pp. 246–255, 2016, doi: 10.1016/j.solener.2016.08.019.
5. S. Pang, H. N. Tsao, X. Feng, and K. Mullen, "Patterned graphene electrodes from solution-processed graphite oxide films for organic field-effect transistors," *Adv. Mater.*, vol. 21, 2009, doi: 10.1002/adma.200803812.
6. A. Bonanni, A. H. Loo, and M. Pumera, "Graphene for impedimetric biosensing," *TrAC Trends Anal. Chem.*, vol. 37, pp. 12–21, Jul. 2012, doi: 10.1016/J.TRAC.2012.02.011.
7. A. Kumar, K. Sharma, and A. R. Dixit, "A review of the mechanical and thermal properties of graphene and its hybrid polymer nanocomposites for structural applications," *J. Mater. Sci.*, vol. 54, no. 8, pp. 5992–6026, Apr. 2019, doi: 10.1007/S10853-018-03244-3/TABLES/4.
8. Q. Abbas *et al.*, "Graphene Synthesis Techniques and Environmental Applications," *Materials (Basel).*, vol. 15, no. 21, Nov. 2022, doi: 10.3390/MA15217804.
9. A. Balachandran, S. P. Sreenilayam, K. Madanan, S. Thomas, and D. Brabazon, "Nanoparticle production via laser ablation synthesis in solution method and printed electronic application - A brief review," *Results Eng.*, vol. 16, 2022, doi: 10.1016/j.rineng.2022.100646.
10. R. M. Altuwirqi, "Graphene Nanostructures by Pulsed Laser Ablation in Liquids: A Review," *Mater. 2022, Vol. 15, Page 5925*, vol. 15, no. 17, p. 5925, Aug. 2022, doi: 10.3390/MA15175925.
11. F. Taccogna, "Nucleation and growth of nanoparticles in a plasma by laser ablation in liquid," *J. Plasma Phys.*, vol. 81, no. 5, p. 495810509, Oct. 2015, doi: 10.1017/S0022377815000793.
12. N. Kumar *et al.*, "Top-down synthesis of graphene: A comprehensive review," *FlatChem*, vol. 27, p. 100224, May 2021, doi: 10.1016/J.FLATC.2021.100224.
13. E. Vaghri, Z. Khalaj, and D. Dorranian, "Investigating the Effects of Different Liquid Environments on the Characteristics of Multilayer Graphene and Graphene Oxide Nanosheets Synthesized by Green Laser Ablation Method," *Diam. Relat. Mater.*, vol. 103, 2020, doi: 10.1016/j.diamond.2020.107697.

14. E. Solati, E. Vaghri, and D. Dorranian, "Effects of wavelength and fluence on the graphene nanosheets produced by pulsed laser ablation," *Appl. Phys. A Mater. Sci. Process.*, vol. 124, no. 11, 2018, doi: 10.1007/s00339-018-2176-2.
15. E. Vaghri and D. Dorranian, "Effects of green laser fluence on the characteristics of graphene nanosheets synthesized by laser ablation method in liquid nitrogen medium," *Opt. Quantum Electron.*, vol. 50, no. 2, pp. 1–11, Feb. 2018, doi: 10.1007/S11082-018-1374-7/FIGURES/7.
16. F. Waag, R. Streubel, B. Gökce, and S. Barcikowski, "Synthesis of gold, platinum, and gold-platinum alloy nanoparticle colloids with high-power megahertz-repetition-rate lasers: the importance of the beam guidance method," *Appl. Nanosci.*, vol. 11, no. 4, pp. 1303–1312, 2021, doi: 10.1007/s13204-021-01693-y.
17. R. Streubel, G. Bendt, and B. Gökce, "Pilot-scale synthesis of metal nanoparticles by high-speed pulsed laser ablation in liquids," *Nanotechnology*, vol. 27, no. 20, 2016, doi: 10.1088/0957-4484/27/20/205602.
18. S. Kudryashov *et al.*, "Polygon-facilitated generation of colloidal gold nanoparticles by multi-MHz ultrashort-pulse laser trains: key optical factors," *Laser Phys. Lett.*, vol. 18, no. 1, 2021, doi: 10.1088/1612- 202X/abd171.
19. A. Nyabadza, M. Vázquez, S. Coyle, B. Fitzpatrick, and D. Brabazon, "Magnesium nanoparticle synthesis from powders via pulsed laser ablation in liquid for nanocolloid production," *Appl. Sci.*, vol. 11, no. 22, 2021, doi: 10.3390/app112210974.
20. I. Gnilitskyi *et al.*, "Laser nanostructuring for diffraction grating based surface plasmon-resonance sensors,"*Nanomaterials*, vol. 11, no. 3, pp. 1–10, 2021, doi: 10.3390/nano11030591.
21. A. Kanitz, J. S. Hoppius, M. del Mar Sanz, M. Maicas, A. Ostendorf, and E. L. Gurevich, "Synthesis of Magnetic Nanoparticles by Ultrashort Pulsed Laser Ablation of Iron in Different Liquids," *ChemPhysChem,*z vol. 18, no. 9, pp. 1155–1164, 2017, doi: 10.1002/cphc.201601252.
22. S. Dittrich, S. Barcikowski, and B. Gökce, "Plasma and nanoparticle shielding during pulsed laser ablation in liquids cause ablation efficiency decrease," *Opto-Electronic Adv.*, vol. 4, no. 1, pp. 1–13, 2021, doi: 10.29026/oea.2021.200072.
23. A. Kanitz, M.-R. Kalus, E. L. Gurevich, A. Ostendorf, S. Barcikowski, and D. Amans, "Review on experimental and theoretical investigations of the early stage, femtoseconds to microseconds processes during laser ablation in liquid-phase for the synthesis of colloidal nanoparticles," *Plasma Sources Sci. Technol.*, vol. 28, no. 10, 2019, doi: 10.1088/1361-6595/ab3dbe.
24. B. Zohuri, "Atmospheric Propagation of High-Energy Laser Beams," in *Directed Energy Weapons*, Cham: Springer International Publishing, 2016, pp. 379–414. doi: 10.1007/978-3-319-31289-7_8.
25. X. Wang *et al.*, "Generation of a large compressive strain wave in graphite by ultrashort-pulse laser irradiation," *Struct. Dyn.*, vol. 6, no. 2, p. 24501, Mar. 2019, doi: 10.1063/1.5089291.
26. L. F. Pires, F. A. M. Cássaro, L. Tech, L. A. A. Pereira, and J. A. T. De Oliveira, "Gamma ray attenuation for determining soil density: Laboratory experiments for environmental physics and engineering courses," *Rev. Bras. Ensino Fis.*, vol. 42, 2020, doi: 10.1590/1806-9126-RBEF-2019-0340.

27. V. V. Semak, A. Gerakis, and M. N. Shneider, “Measurement of temperature dependent absorption coefficient of water at 1064nm wavelength,” *AIP Adv.*, vol. 9, no. 8, p. 85016, Aug. 2019, doi: 10.1063/1.5085746/127779.
28. P. Wagener, A. Schwenke, B. N. Chichkov, and S. Barcikowski, “Pulsed laser ablation of zinc in tetrahydrofuran: Bypassing the cavitation bubble,” *J. Phys. Chem. C*, vol. 114, no. 17, pp. 7618–7625, May 2010, doi: 10.1021/JP911243A/SUPPL_FILE/JP911243A_SI_001.PDF.